Biogeosciences Discuss., 11, 15991–16032, 2014
www.biogeosciences-discuss.net/11/15991/2014/
doi:10.5194/bgd-11-15991-2014

Biogeosciences
Discussions
Open Access

Carbon export in the naturally iron-fertilized Kerguelen area of the Southern Ocean based on the ^{234}Th approach

F. Planchon[1], **D. Ballas**[2], **A.-J. Cavagna**[2], **A. R. Bowie**[3,4], **D. Davies**[4], **T. Trull**[3,4,5], **E. Laurenceau**[3], **P. Van Der Merwe**[4], **and F. Dehairs**[2]

[1]Laboratoire des Sciences de l'Environnement Marin (LEMAR), Université de Brest, CNRS, IRD, UMR 6539, IUEM, Technopôle Brest Iroise, Place Nicolas Copernic, 29280 Plouzané, France
[2]Vrije Universiteit Brussel, Analytical, Environmental and Geo-Chemistry and Earth System Sciences, Brussels, Belgium
[3]Institute for Marine and Antarctic Studies, University of Tasmania, Hobart, 7001, Australia
[4]Antarctic Climate and Ecosystems Cooperative Research Centre, Hobart, 7001, Australia
[5]CSIRO Marine and Atmospheric Research, Hobart, 7001, Australia

Received: 3 October 2014 – Accepted: 13 October 2014 – Published: 25 November 2014

Correspondence to: F. Planchon (frederic.planchon@univ-brest.fr)

Published by Copernicus Publications on behalf of the European Geosciences Union.

Abstract

The Kerguelen Plateau region in the Indian sector of the Southern Ocean supports annually a large-scale phytoplankton bloom which is naturally fertilized with iron. As part of the second KErguelen Ocean and Plateau compared Study expedition (KEOPS2) in austral spring (October–November 2011), we examined upper-ocean Particulate Organic Carbon (POC) export using the ^{234}Th approach. We aimed at characterizing the spatial and the temporal variability of POC export production at high productivity sites over and downstream the Kerguelen plateau. Export production is compared to a High Nutrient Low Chlorophyll area upstream of the plateau in order to assess the impact of iron-induced productivity on the vertical export of carbon.

Deficits in ^{234}Th activities relative to its parent nuclide ^{238}U were observed at all stations in surface waters, indicating that scavenging by particles occurred during the early stages of the phytoplankton bloom. ^{234}Th export was lowest at reference station R-2 (412 ± 134 dpm m^{-2} d^{-1}) and highest inside a permanent meander of the Polar Front (PF) at stations E (1995 ± 176 dpm m^{-2} d^{-1}, second visit E-3) where a detailed time series was obtained as part of a pseudo-lagrangian study. ^{234}Th export over the central plateau was relatively limited at station A3 early (776 ± 171 dpm m^{-2} d^{-1}, first visit A3-1) and late in the survey (993 ± 223 dpm m^{-2} d^{-1}, second visit A3-2), but it was higher at high biomass stations TNS-8 (1372 ± 255 dpm m^{-2} d^{-1}) and E-4W (1068 ± 208 dpm m^{-2} d^{-1}) in waters which could be considered as derived from plateau. Limited ^{234}Th export of 973 ± 207 dpm m^{-2} d^{-1} was also found in the northern branch of the Kerguelen bloom located downstream of the island, north of the PF (station F-L). The ^{234}Th results support that Fe fertilization increased particle export in all iron fertilized waters. The impact was greatest in the recirculation feature (3–4 fold at 200 m depth), but more moderate over the central Kerguelen plateau and in the northern plume of the Kerguelen bloom (~ 2-fold at 200 m depth).

The C : Th ratio of large (> 53 µm) potentially sinking particles collected via sequential filtration using in situ pumping (ISP) systems were used to convert the

^{234}Th flux into a POC export flux. The C : Th ratios of sinking particles were highly variable (range: 3.1±0.1–10.5±0.2 µmol dpm^{-1}) with no clear site related trend, despite the variety of ecosystem responses in the fertilized regions. C : Th ratios showed a decreasing trend between 100 and 200 m depth suggesting preferential loss of carbon relative to ^{234}Th possibly due to heterotrophic degradation and/or grazing activity. Comparison of the C : Th ratios within sinking particles obtained with the drifting sediment traps showed in most cases very good agreement to those collected via ISP deployments (> 53 µm particles).

Carbon export production varied between 3.5 ± 0.9 mmol m^{-2} d^{-1} and 11.8 ± 1.3 mmol m^{-2} d^{-1} from the upper 100 m and between 1.8 ± 0.9 mmol m^{-2} d^{-1} and 8.2 ± 0.9 mmol m^{-2} d^{-1} from the upper 200 m. Highest export production was found inside the PF meander with a range of 5.4±0.7 mmol m^{-2} d^{-1} to 11.8±1.1 mmol m^{-2} d^{-1} at 100 m depth decreasing to 5.3 ± 1.0 mmol m^{-2} d^{-1} to 8.2 ± 0.8 mmol m^{-2} d^{-1} at 200 m depth over the 19 day survey period. The impact of Fe fertilization is highest inside the PF meander with 2.9- up to 4.5-fold higher carbon flux at 200 m depth in comparison to the HNLC control station. The impact of Fe fertilization was significantly less over the central plateau (stations A3 and E-4W) and in the northern branch of the bloom (station F-L) with 1.6- up to 2.0-fold higher carbon flux compared to the reference station R. Export efficiencies (ratio of export to primary production) were particularly variable with relatively high values in the recirculation feature (6–27 %) and low values (1–5 %) over the central plateau (station A3) and north of the PF (station F-L) indicating spring biomass accumulation. Comparison with KEOPS1 results indicated that carbon export production is much lower during the onset of the bloom in austral spring in comparison to the peak and declining phase in late summer.

1 Introduction

Nutrient limitation is an essential control of upper-ocean productivity (Moore et al., 2013) and affects the associated uptake of carbon and its transfer to the deep ocean as sinking particulate organic matter. Attention has focused on iron (Fe) as a limiting nutrient since the *iron hypothesis* of Martin (1990), who suggested that increased iron supply to the Southern Ocean (SO) during the last glacial maximum could have contributed to the drawdown of atmospheric CO_2 by stimulating the oceanic biological pump. For the present-day ocean, iron limitation is now validated for several high-nutrient-low-chlorophyll (HNLC) regions, including the Southern Ocean (Boyd et al., 2007, 2000; Coale et al., 2004; Martin et al., 1990, 1991; Sedwick et al., 1999; Smetacek et al., 2012). However, it is still under debate whether the positive growth response of phytoplankton due to iron addition results in enhanced export of biogenic particles and contributes to the long-term sequestration of carbon. This remains central to understanding the role of iron on the oceanic carbon cycle and ultimately on the past and future climate of the Earth.

Mesoscale iron addition experiments have revealed no clear trend in carbon export. Export fluxes estimated during SOIREE (Polar waters south of Australia), SAGE (subpolar waters south of New Zealand), EisenEx (Atlantic polar waters) and LOHAFEX (South-Atlantic waters) report no major differences between the Fe-fertilized patch and the adjacent control site (Buesseler et al., 2004, 2005; Martin et al., 2013; Nodder et al., 2001). By contrast, the experiments SOFEX-South (polar waters south of New Zealand) and EIFEX (Atlantic polar waters south of Africa) showed increased vertical flux of particulate organic carbon due to iron addition (Buesseler et al., 2005; Jacquet et al., 2008; Smetacek et al., 2012). Enhanced export appears associated with experiments carried out (1) in high silicic acid waters south of the Antarctic Polar Front (PF) allowing fast-sinking, large diatoms to develop under low grazing pressure and (2) over a survey period sufficiently long to cover the time lag between the bloom development and the export event. However, the key results obtained with purposeful

BGD
11, 15991–16032, 2014

iron addition still differ and are difficult to scale up to regional and seasonal scales (Boyd et al., 2007).

Alternatives to short-term artificial experiments are the large and persistent phytoplankton blooms that develop annually in the vicinity of sub-Antarctic islands (Blain et al., 2007; Borrione and Schlitzer, 2013; Pollard et al., 2009) and close to the Antarctic continent (Alderkamp et al., 2012; Zhou et al., 2013) due to natural iron supply. These particular settings represent large scale natural laboratories, where the role of Fe on ecosystems ecology, productivity, structure, and associated export can be monitored over an entire seasonal cycle. Two previous important field studies were carried out in natural Fe-fertilized areas, the CROZet natural iron bloom and EXport experiment (CROZEX, 2004–2005) (Pollard et al., 2009), and the KErguelen Ocean and Plateau compared study (KEOPS, 2005) (Blain et al., 2007). CROZEX studied the Crozet Islands region located in sub-Antarctic waters of the Indian Ocean where a bloom occurs north of the Islands in October/November followed by a secondary bloom in January. CROZEX results confirmed that the bloom is fueled with iron from the Crozet Island (Planquette et al., 2007) and that phytoplankton uptake rates are much larger in the bloom area than in the HNLC control area (Lucas et al., 2007; Seeyave et al., 2007). For carbon export, the primary bloom results in ~ 3-fold higher flux at the Fe-fertilized site than at the control site, and for the secondary bloom, no substantial differences are reported (Morris et al., 2007). Sinking particles collected by a neutrally buoyant sediment trap (PELAGRA) were dominated by diatom cells of various species and size indicating a pronounced contribution of primary producers to the export (Salter et al., 2007).

The second study (KEOPS) focused on the high productivity area of the Kerguelen Island in the Indian sector of the SO. The Kerguelen bloom has two main features, a northern branch that extends northeast of the island north of the PF (also called the plume), and a larger bloom covering ~ 45 000 km^2 south of the PF and largely constrained to the shallow bathymetry of the Kerguelen Plateau (< 1000 m) (Mongin et al., 2008). In austral summer 2004–2005, the bloom started in early November,

BGD
11, 15991–16032, 2014

peaked in December and January, and then rapidly declined in February (Blain et al., 2007). Fe fertilization over the plateau was demonstrated during KEOPS and attributed to vertical exchanges between the surface and the deep iron-rich reservoir existing above the plateau (Blain et al., 2008). The waters in the bloom showed higher biomass, greater silicate depletion, and important CO_2 drawdown compared to the control site (Blain et al., 2007; Jouandet et al., 2008; Mosseri et al., 2008). Carbon export in the Fe-fertilized area in comparison to HNLC waters was 2-fold higher as estimated using the ^{234}Th proxy (Savoye et al., 2008), and 3-fold higher based on a seasonal dissolved inorganic carbon (DIC) budget (Jouandet et al., 2008). Direct observations of sinking particles using polyacrylamide gel traps indicates a dominant fraction of fecal pellets and fecal aggregates and suggests a strong influence of particle repackaging by grazers during the late stage of the Kerguelen bloom (Ebersbach and Trull, 2008). The unprecedented results obtained from CROZEX and KEOPS clearly highlight the crucial role of Fe on natural ecosystems and demonstrate the stimulation of the biological carbon pump in the SO resulting in an enhanced CO_2 sink and carbon export at depth.

The KEOPS2 project was designed to improve the spatial and temporal coverage of the Kerguelen region. KEOPS2 was carried out in austral spring to document the early stages of the bloom and to complement results of KEOPS1 obtained in summer during the peak and decline of the bloom. The principal aims were to better constrain the mechanism of Fe supply to surface waters and to determine the response of ecosystems to Fe fertilization including the impact on vertical export of carbon. The sampling strategy covered two distinct areas, the principal bloom already investigated during KEOPS1 and located over the central plateau, and the plume downstream to the east of the Island and north of the PF.

In this study, we report upper-ocean particulate organic carbon (POC) export production estimated using the ^{234}Th-based approach (Cochran and Masqué, 2003). POC fluxes at 100, 150 and 200 m depth were inferred from total ^{234}Th export fluxes estimated from ^{234}Th deficit in surface waters by applying the modeling approach of Savoye et al. (2006) for the ^{234}Th activity balance. ^{234}Th export fluxes were then converted into POC fluxes using POC / ^{234}Th ratio of large (> 53 µm) potentially sinking particles at the depth of export. Upper-ocean ^{234}Th and carbon export obtained in HNLC and Fe-enriched waters were used to assess the impact of natural fertilization on the vertical transfer of carbon. ^{234}Th-derived fluxes were compared to free-drifting sediment and polyacrylamide gel traps data (Laurenceau et al., 2014). Using primary production estimates (Cavagna et al., 2014) we examine spatial and temporal variations in export efficiency during the survey. Finally, using KEOPS1 results, early and late bloom conditions are compared.

2 Material and method

2.1 Study area and sampling strategy

The KEOPS2 cruise took place between October and November 2011 on board the R/V *Marion Dufresne*. The studied region encompasses the Kerguelen plateau located between Kerguelen and Heard Island, and the deeper off-shore basin to the east of the island (Fig. 1). Details of the large-scale circulation in this area can be found elsewhere (Park et al., 2008b). Briefly, the Kerguelen plateau represents a major barrier to the eastward flow of the Antarctic Circumpolar Current (ACC). The ACC is divided into two branches with the most intense flow passing to the north of the island and associated to the Sub-Antarctic Front (SAF). The second branch is associated to the PF and passes south of the island. When crossing the plateau the southern branch turns back north and forms a large meander isolating a mesoscale recirculation structure south of the PF (Fig. 1).

The sampling strategy aimed at characterizing the spatial and the temporal variability of high productivity sites located on and off the plateau. The survey included two transects from south to north (TNS-1 to TNS-10) and from west to east (TEW-1 to TEW-8) for physics and stock parameters, and nine process stations (R-2, A3-1, A3-2, E-1, E-3, E-4W, E-4E, E-5, and F-L) where more intensive sampling including large

BGD
11, 15991–16032, 2014

volume in situ filtration and sediment trap deployments were carried out. For this study, 14 stations were investigated including five transects stations (TNS-8, TNS-6, TNS-1, E-2, and TEW-8) sampled for total ^{234}Th activity and nine process stations where total ^{234}Th, particulate ^{234}Th and POC profiles obtained simultaneously allowed to estimate POC export production. Sediment traps deployed and successfully recovered at four process stations were also determined for ^{234}Th activity. Process stations were carried out in four distinct areas showing different characteristics (see Fig. 1):

- The reference station (R-2) was chosen in HNLC waters upstream of the island in a non-Fe-fertilized area.
- The shallow central plateau was sampled at station A3, which corresponds to the plateau bloom reference station of KEOPS1. Station A3 was sampled twice (A3-1 and A3-2) over a period of 27.7 days (20 October–16 November).
- The northern branch of the bloom, which develops north of the PF in the Polar Front Zone (PFZ), was sampled at station F-L (6 November).
- The recirculation feature in the PF meander (station E) received detailed attention with four successive visits (E-1, E-3, E-4E, and E-5) as part of a pseudo-lagrangian time-series over 19.6 days. In the same area, a highly productive station (E4W) located on the western edge of the recirculation feature and close to the jet of the PF was sampled but excluded from the pseudo-lagrangian study.

2.2 Total ^{234}Th activities

Total ^{234}Th activities were obtained from 4 L seawater samples collected from 12 L Niskin bottles. For transect stations, 13 depths were sampled between the surface and 20–90 m above the seafloor. For plateau station A3, samples were collected at 11 depths between the surface and 30–80 m above the seafloor. For deep stations (R, E-1, E-3, E-4E, E-4W, E-5, F-L), 14 depths were sampled between the surface and

BGD
11, 15991–16032, 2014

900 m, and two deep water samples (1000–2000 m) were systematically collected for calibration purposes (except at E-4W).

Seawater samples were processed for total ^{234}Th activity measurement following the double-spike procedure developed by Pike et al. (2005) and modified as per Planchon et al. (2013). Briefly, samples were acidified with nitric acid (pH 2), spiked with ^{230}Th yield tracer, and left for 12 h equilibration before co-precipitation with MnO_2 (pH 8.5). Co-precipitated samples were filtered on high-purity quartz microfiber filters (QMA, Sartorius; nominal pore size = 1 µm; Ø 25 mm), dried overnight and mounted on nylon filter holders for beta counting. Samples were counted twice on board using a low level beta counter (RISØ, Denmark) and measurement was stopped when counting uncertainty was below 2 % (RSD). Residual beta activity was measured for each sample after a delay of 6 ^{234}Th half-lives (~ 6 months) and was subtracted from the gross counts obtained on-board.

After background counting, all samples were processed for ^{234}Th recovery using ^{229}Th as a second yield tracer and with a simplified procedure described elsewhere (Planchon et al., 2013). Briefly, MnO_2 co-precipitates were dissolved in 10 mL of a 8 M HNO_3/10 % H_2O_2 solution, heated overnight and filtered using Acrodisc 0.2 µm syringe filters. Determination of ^{230}Th / ^{229}Th ratios was carried out on high purity water diluted samples (10 to 20 times) by HR-ICP-MS (Element2, Thermo Scientific). The overall precision of ^{230}Th / ^{229}Th ratio measurements was 1.8 % (RSD) using triplicate samples and multiple standards analyzed over several analytical sessions. Average ^{234}Th recovery was 88 ± 11 % ($n = 200$). Uncertainties on total ^{234}Th activity were estimated using error propagation law and represent 0.07 dpm L^{-1} on average. SD of the mean ^{234}Th / ^{238}U ratio obtained for deep waters (> 1000 m) was 0.03 dpm L^{-1} ($n = 19$). ^{238}U activity (dpm L^{-1}) was calculated using the relationship ^{238}U (±0.047) = (0.0786 ± 0.0045) × S – (0.315 ± 0.158) (Owens et al., 2011).

BGD
11, 15991–16032, 2014

2.3 ^{234}Th flux

^{234}Th export fluxes were calculated using a 1-D box model, which accounts for total ^{234}Th mass balance. Detailed equations can be found elsewhere (Savoye et al., 2006). ^{234}Th export flux was estimated at 100, 150, and 200 m depth in order to account for variations in the depth distributions of the ^{234}Th deficits, and also to allow comparison with KEOPS1 study (Savoye et al., 2008). At all stations, ^{234}Th flux was estimated under steady state assumption (SS), i.e. considering constant total ^{234}Th activity over time and neglecting advective and diffusive flux of ^{234}Th. For re-visited stations (A3 and E stations), ^{234}Th flux was also estimated under non-steady state assumption (NSS). At A3, the NSS model was applied for the second visit with a time delay of 27.7 days. At E stations, NSS ^{234}Th export flux was estimated when the time delay was greater than one week as recommended by Savoye et al. (2006). Consequently, the NSS calculation was carried out only at E-4E (14.6 days) and E-5 (19.6 days). The revisited stations E-2 and E-4W were not considered part of the pseudo-lagrangian study at the E study site and were excluded from the NSS calculation.

In order to check the assumption that physical transport did not impact the ^{234}Th budget, the vertical diffusive flux (Vz) was estimated using the vertical gradient of ^{234}Th activity and a range of vertical diffusivity coefficients Kz between 10^{-4} m^2 s^{-1} and 10^{-5} m^2 s^{-1} calculated from the Shih model (Park et al., 2014). This range of Kz values for KEOPS2 is much lower than for KEOPS1 (4×10^{-4} m^2 s^{-1}) obtained using Osbourn model (Park et al., 2008a). Vz was calculated using total ^{234}Th activities instead of the dissolved ^{234}Th (total ^{234}Th-particulate ^{234}Th) because of a poor vertical resolution of particulate ^{234}Th data in the first 200 m. For all stations, the diffuse flux (Vz) estimated at 100, 150, and 200 m depth was always below 50 dpm m^2 d^{-1} and represents a negligible contribution to the particle-associated export flux.

BGD
11, 15991–16032, 2014

2.4 Particulate ^{234}Th and POC

Suspended particulate matter was collected at nine process stations for particulate ^{234}Th and POC via large-volume (150–1000 L) in-situ filtration systems (Challenger Oceanics and McLane WTS6–1-142LV pumps) equipped with 142 mm diameter filter holders. Two size classes of particles (> 53 and 1–53 µm) were collected via sequential filtration across a 53 µm mesh nylon screen (SEFAR-PETEX®) and a 1 µm pore size quartz fiber filter (QMA, Sartorius). To limit C and N blanks, the filters were pre-conditioned prior to sampling. For large particles (> 53 µm), the PETEX screens were soaked in HCl 5 %, rinsed with Milli-Q water, dried at ambient temperature in a laminar flow hood and stored in clean plastic bags. QMA filters were pre-combusted and acid cleaned following Bowie et al. (2010).

After collection, filters were subsampled under clean room conditions with acid cleaned ceramic scissors for PETEX screen and a 25 mm Plexiglas punch for QMA. For large particles, one fourth of the 142 mm nylon screen was dedicated to ^{234}Th and POC. Particles were re-suspended in filtered seawater in a laminar flow clean hood and collected on 25 mm diameter silver (Ag) filters (1.0 µm porosity). For small particles, two 25 mm diameter punches were subsampled from the 142 mm QMA filters. Ag and QMA filters were dried overnight and mounted on nylon filter holders covered with Mylar and Al foil for beta counting. As for total ^{234}Th activity, particulate samples were counted twice on board until the RSD was below 2 %. The procedure was similar for sediment traps samples. Sediment traps samples were re-suspended in filtered seawater, collected on Ag filters, dried, and mounted on nylon filter holder. Residual beta activity was measured in the home-based laboratory after six ^{234}Th half-lives (∼ 6 months) and was subtracted from the on-board measured values.

Following beta counting, particulate samples (QMA and Ag filters) were processed for POC measurement by Elemental Analyzer – Isotope Ratio Mass Spectrometer (EA-IRMS). Samples were dismounted from filters holders and fumed under HCl vapor during 4 h inside a glass desiccator, to remove the carbonate phase. After overnight drying at 50 °C, samples were packed in silver cups and analyzed with a Carlo Erba NA 1500 elemental analyzer configured for C analysis and coupled on-line via a Con-Flo III interface to a Thermo-Finnigan Delta V isotope ratio mass spectrometer. Acetanilide standards were used for calibration. C blanks were 1.46 µmol for Ag filters and 0.52 µmol for 25 mm QMA punch. Results obtained for two size-segregated POC fractions (> 53 and 1–53 µm) are reported in Appendix 2 in the Supplement along with particulate ^{234}Th activity measured on the same samples.

3 Results

3.1 ^{234}Th activity profiles

The complete dataset of total ^{234}Th ($^{234}Th_{tot}$), ^{238}U activities (dpm L^{-1}) and associated $^{234}Th/^{238}U$ ratios can be found in Supplementary Appendix 1. At all stations, the deficit of $^{234}Th_{tot}$ relative to ^{238}U was observed in surface waters ($^{234}Th/^{238}U$ = 0.78–0.95). $^{234}Th_{tot}$ activities increased progressively with depth and were back to equilibrium with ^{238}U at variable depths according to station: above 100 m at R, TNS-1 and F-L, between 100 and 150 m at A3-1, TEW-8, E-4E and E-4W and between 150 and 200 m at TNS-6, TNS-8, E-1, E-2, E-3, E-5 and A3-2. Such a pattern is typically encountered in the open-ocean (Le Moigne et al., 2013) including the Southern Ocean (Buesseler et al., 2001; Cochran et al., 2000; Morris et al., 2007; Planchon et al., 2013; Rutgers van der Loeff et al., 2011; Savoye et al., 2008) and indicates scavenging of ^{234}Th with sinking particles. Figure 2 shows the early season trend in $^{234}Th/^{238}U$ ratios observed along the south to north transect from the central plateau (first visit to A3, A3-1), on the downward slope of the plateau (TNS-8), across the E stations (TNS-6) to the warmer less-saline PFZ waters north of the PF (TNS-1). Surface $^{234}Th/^{238}U$ ratios varied from 0.92 (A3-1) to 0.85 (TNS-8) and indicates that export of particles had already occurred early at this time in the season (mid-October). Deficit was higher inside the PF meander ($^{234}Th/^{238}U$ ratios of 0.85 to 0.88 at TNS-8 and TNS-6, respectively)

BGD
11, 15991–16032, 2014

Carbon export in the naturally iron-fertilized Kerguelen area of the Southern Ocean

F. Planchon et al.

and north of the PF ($^{234}Th/^{238}U = 0.88$ at TNS-1) compared to the shallow central plateau ($^{234}Th/^{238}U = 0.92$ at A3-1). Over the plateau, bottom water (~ 50–80 m above seafloor) exhibited the lowest $^{234}Th/^{238}U$ ratios (0.75). This pattern has already been documented (Savoye et al., 2008) and supports ^{234}Th removal due to sediment re-suspension.

At process stations, $^{234}Th_{tot}$ profiles were obtained in combination with particulate ^{234}Th ($^{234}Th_p$) for two size fractions (1–53, > 53 µm). Results obtained in the different areas are shown in Fig. 3 for $^{234}Th_{tot}$, $^{234}Th_p$ (sum of the two size fractions), and dissolved ^{234}Th (total – particulate, $^{234}Th_d$) along with ^{238}U activity (dpm L^{-1}) deduced from salinity using the equation of Owens et al. (2011). The average $^{234}Th_{tot}$ within the first 100 m exhibited a relatively small variability over the KEOPS2 area with 2.21 ± 0.10 dpm L^{-1} ($n = 4$, $^{234}Th/^{238}U = 0.95 \pm 0.04$) at R-2, 2.18 ± 0.05 dpm L^{-1} ($n = 5$, $^{234}Th/^{238}U = 0.93 \pm 0.02$) at A3-1, 2.07 ± 0.20 dpm L^{-1} ($n = 4$, $^{234}Th/^{238}U = 0.89 \pm 0.08$) at F-L, and 1.98 ± 0.03 dpm L^{-1} ($n = 4$, $^{234}Th/^{238}U = 0.84 \pm 0.01$) at E-1. In contrast, surface $^{234}Th_p$ activity, which reflects particle concentration, was subject to larger variation. $^{234}Th_p$ activity was low at R-2 (0.33 dpm L^{-1}) and at A3-1 (0.29 dpm L^{-1}), intermediate at E-1 (0.50 dpm L^{-1}) and highest at F-L (0.90 dpm L^{-1}). Over the course of the survey, averaged $^{234}Th_{tot}$ activity within the first 100 m remained remarkably stable over the plateau, with 2.13 ± 0.06 dpm L^{-1} ($n = 3$, $^{234}Th/^{238}U = 0.90 \pm 0.03$) at A3-2 (27.7 days later), and in the PF meander, with 1.91 ± 0.07 dpm L^{-1} ($n = 4$, $^{234}Th/^{238}U = 0.82 \pm 0.03$) at E-3 (4.5 days later) and 1.92 ± 0.02 dpm L^{-1} ($n = 4$, $^{234}Th/^{238}U = 0.82 \pm 0.01$) at E-5 (19.6 days later). For the particulate phase, the situation was different. At A3, $^{234}Th_p$ increased from 0.29 to 0.66 dpm L^{-1} between the two visits. At site E, $^{234}Th_p$ varied from 0.50 to 0.70 dpm L^{-1} between the first (E-1) and the last (E-5) visit, suggesting an increase in particle concentrations in surface waters at both A3 and E stations.

BGD
11, 15991–16032, 2014

3.2 ^{234}Th flux

Total ^{234}Th activity profiles were used for estimating export fluxes based on SS and NSS assumptions. Cumulated export fluxes of total ^{234}Th are presented in Fig. 4. Using the SS calculation, ^{234}Th export flux from the first 100 m ranged from 412 ± 134 dpm m^{-2} d^{-1} at R-2 to 1326 ± 110 dpm m^{-2} d^{-1} at E-3. ^{234}Th export flux increased below 100 m depth except at station R-2 and north of the PF (stations F-L, TEW-8, and TNS-1) where ^{234}Th was back to equilibrium with ^{238}U above 100 m. At 200 m depth, ^{234}Th export flux reached 993 ± 200 dpm m^{-2} d^{-1} at A3-2, 1372 ± 255 dpm m^{-2} d^{-1} at TNS-8, and between 1296 ± 193 and 1995 ± 176 dpm m^{-2} d^{-1} at E stations. At A3, the NSS ^{234}Th export flux was 736±186 dpm m^{-2} d^{-1} at 100 m and 1202±247 dpm m^{-2} d^{-1} at 200 m and compares well with SS export. At E stations, NSS export from the first 100 m were 911 ± 242 at E-4E and 1383 ± 177 dpm m^{-2} d^{-1} at E-5 and also compares well with SS fluxes. Between 100 and 200 m, NSS ^{234}Th flux increased at E-5 (2034 ± 299 dpm m^{-2} d^{-1}) and decreased at E-4E (520 ± 402 dpm m^{-2} d^{-1}). In addition to water-column data, export of ^{234}Th was determined from sediment traps deployed at 200 m depth (see Fig. 4 and Table 1). Details of trap deployments carried out at E-1, E-3, E-5, and A3-2 can be found elsewhere (Laurenceau et al., 2014). Export of ^{234}Th measured in trap samples ranged from 506 ± 21 dpm m^{-2} d^{-1} at A3-2 to 1129 ± 177 dpm m^{-2} d^{-1} at E-3 and represented ~ 50 % of the SS and NSS export flux determined from ^{234}Th$_{tot}$ activity profiles.

3.3 C : Th ratio of particles

At process stations, particulate ^{234}Th activities and POC were obtained in two size fractions of particles (1–53, > 53 µm). Profiles of POC to ^{234}Th ratios (C : Th) are shown in Fig. 5. C : Th ratios were highly variable ranging from 21.5 to 1.8 µmol dpm^{-1} in 1–53 µm particles and from 12.5 to 1.0 µmol dpm^{-1} in > 53 µm particles. For both size classes, C : Th ratios were high in surface waters (0–150 m) with a range of 9.6–6.3 µmol dpm^{-1} at R, 13.1–6.9 at A3, and 11.4–5.7 µmol dpm^{-1} at E stations with

BGD
11, 15991–16032, 2014

no clear site related trend. For open-ocean stations, C : Th ratios decreased rapidly with depth for the two size classes of particles and reached relatively constant values in the mesopelagic zone with 2.8–4.8 µmol dpm^{-1} at R-2, 2.6–4.5 µmol dpm^{-1} at E stations, and 1.6–2.7 µmol dpm^{-1} at F-L. According to particle size C : Th ratios showed different trends. At R-2, E-1, E-3, E-4W and E-5, C : Th ratios were comparable in small and large particles. At plateau stations A3-1 and A3-2, and to a lesser extent at E-4E, C : Th ratios increased with decreasing size of particles.

3.4 C : Th ratio of sinking particles

To estimate the POC export flux using the ^{234}Th-based approach, the C : Th ratio of sinking particles needs to be determined at the depth of export (Buesseler et al., 1992). Assuming the larger particle size class as representative of the sinking material (Buesseler et al., 2006), we used the C : Th ratios of > 53 µm particles to convert ^{234}Th fluxes into POC fluxes. C : Th ratios were estimated at fixed depths of 100, 150, and 200 m and results are listed in Table 1 and plotted in Fig. 5. For A3-1, A3-2, E-1, E-3, E-4W, and E-5, C : Th ratios of sinking particles were estimated from linear interpolation of measured C : Th ratios. At R-2, the C : Th ratio at 100 m represents the average ratio measured between 25 and 110 m. At F-L, the 100 m C : Th ratio was taken equal to the value at 130 m. For E-4E, C : Th of large particles were measured directly at the depths of 100, 150 and 200 m and were not interpolated. As illustrated in Fig. 5 and in Table 1, C : Th ratios of sinking particles at 200 m estimated using ISP samples showed a good agreement with sediment trap data within uncertainty (3–6 % and 18–46 % RSD for ISP and trap C : Th ratios, respectively).

3.5 POC export flux

POC export fluxes were estimated at 100 m (EP100), 150 m (EP150), and 200 m (EP200) by multiplying the corresponding ^{234}Th export flux with the C : Th ratio of sinking particles at the depth of export. Results are listed in Table 1. EP100 fluxes

BGD
11, 15991–16032, 2014

estimated with the SS model were lowest at A3-1 ($3.5 \pm 0.9\,\mathrm{mmol\,m^{-2}\,d^{-1}}$) and at R-2 ($3.8 \pm 1.2\,\mathrm{mmol\,m^{-2}\,d^{-1}}$) and highest at E-1 with $11.8 \pm 1.3\,\mathrm{mmol\,m^{-2}\,d^{-1}}$. The EP100 flux at F-L was $4.1 \pm 0.6\,\mathrm{mmol\,m^{-2}\,d^{-1}}$ and was similar to the value for the control station R-2 and the plateau station A3. In the PF meander, EP100 remained stable between the two first visits (E-3) with $11.8 \pm 1.1\,\mathrm{mmol\,m^{-2}\,d^{-1}}$, but decreased at the third visit (E-4E) to $5.4 \pm 0.7\,\mathrm{mmol\,m^{-2}\,d^{-1}}$ at E4-E, and increased to $7.7 \pm 0.7\,\mathrm{mmol\,m^{-2}\,d^{-1}}$ at the last visit (E-5). Station E-4W, not included in the time series, had an EP100 of $6.7 \pm 0.9\,\mathrm{mmol\,m^{-2}\,d^{-1}}$ very similar to E-4E on the eastern edge of the PF meander. At 200 m, export fluxes ranged between $1.8 \pm 0.9\,\mathrm{mmol\,m^{-2}\,d^{-1}}$ (R-2) and $8.2 \pm 0.8\,\mathrm{mmol\,m^{-2}\,d^{-1}}$ (E-3). At the re-visited stations, carbon export production was also estimated using the NSS model approach. NSS EP100 varied from $4.6 \pm 1.3\,\mathrm{mmol\,m^{-2}\,d^{-1}}$ (E-4E) to $8.4 \pm 1.1\,\mathrm{mmol\,m^{-2}\,d^{-1}}$ (E-5). Within uncertainty, NSS EP100 were similar (E-5 and E-4E) or higher (A3) in comparison to SS EP100. Export production determined at 200 m depth with the ^{234}Th proxy could be directly compared to fluxes estimated with sediment traps deployed at the same depth (Table 1). Traps fluxes in comparison to EP200 were in very good agreement within uncertainties at E-1 ($7.0 \pm 2.3\,\mathrm{mmol\,m^{-2}\,d^{-1}}$ and $7.7 \pm 1.0\,\mathrm{mmol\,m^{-2}\,d^{-1}}$ for trap and ^{234}Th-based fluxes, respectively) and A3-2 ($2.2 \pm 0.7\,\mathrm{mmol\,m^{-2}\,d^{-1}}$ and $3.1 \pm 0.6\,\mathrm{mmol\,m^{-2}\,d^{-1}}$ for trap and ^{234}Th-based fluxes, respectively), and 1.7-fold and 3.3-fold lower at E-3 and E-5, respectively.

4 Discussion

The principal aim of this study was to estimate how natural Fe fertilization affects carbon export at high productivity sites over and off plateau during the early stages of the bloom. In the following sections, results obtained with the ^{234}Th-based approach and summarized in Fig. 6 are discussed according to the four distinct zones investigated during the survey (control station R-2, North of the Polar Front station F-L, Plateau station A3, and PF meander stations E).

BGD
11, 15991–16032, 2014

4.1 Reference site R

At reference station R-2, the observed export production at 100 m of $3.8 \pm 1.2\,\mathrm{mmol\,m^{-2}\,d^{-1}}$ is very small and reflects mainly a small and shallow export of ^{234}Th ($412 \pm 134\,\mathrm{dpm\,m^{-2}\,d^{-1}}$ at 100 m). Low export is consistent with the HNLC conditions at station R, where high concentrations of nitrate (25 µM), silicic acid (12–13 µM) (Blain et al., 2014) and very low biomass (Lasbleiz et al., 2014) and iron levels are observed in surface waters (Queroue et al., 2014). Biomass at station R-2 appears to be dominated by small size, slow growing phytoplankton (Trull et al., 2014), which offers a limited potential for export. This feature is reflected in the partitioning of POC and $^{234}Th_p$ with ~ 90 % being associated with the small (1–53 µm) size fraction between 25 and 110 m depth. C : Th ratios of particles show no variation with particle size (Fig. 5) and suggest that large sinking particles may be a result of aggregation process (Buesseler et al., 2006). This is supported by gel trap observations, revealing that phytodetrital aggregates are an important fraction of sinking material between 110 and 400 m depth (Laurenceau et al., 2014).

The flux obtained at the KEOPS2 reference station is similar to results obtained during the first leg of CROZEX (November–December 2004) at control sites M2 and M6, with carbon export of $4.9 \pm 2.7\,\mathrm{mmol\,m^{-2}\,d^{-1}}$ and $5.8 \pm 3.9\,\mathrm{mmol\,m^{-2}\,d^{-1}}$, respectively (Morris et al., 2007). Our value for C export is however much lower than the flux obtained in summer at the KEOPS1 control site C11 ($12.2 \pm 3.3\,\mathrm{mmol\,m^{-2}\,d^{-1}}$) (January–February 2005) (Savoye et al., 2008) or during the second Leg of CROZEX (December 2004–January 2005) with $18.8 \pm 3.4\,\mathrm{mmol\,m^{-2}\,d^{-1}}$ at M2 and $14.4 \pm 3.0\,\mathrm{mmol\,m^{-2}\,d^{-1}}$ at M6 (Morris et al., 2007).

Comparison between export and production can be addressed using the ThE ratio defined as the ratio of EP100 to Net Primary Production (NPP) (Buesseler, 1998). During KEOPS2, NPP was estimated from short-term (24 h) deck board ^{13}C-HCO_3^- incubation experiments (Cavagna et al., 2014). For the reference station R-2, ThE ratio was 34 % and indicates a relatively efficient carbon pump despite the limited magnitude of export and uptake (11.2 $mmol\,m^{-2}\,d^{-1}$). This value falls in the range of most literature data for the Southern Ocean, for which ThE ratio is generally high (> 10 %) (Savoye et al., 2008). Reasons for this high efficiency can be numerous and may involve, for instance, the Fe limitation as observed during KEOPS1 at C11 (ThE = 58 %) (Savoye et al., 2008) or in the Antarctic zone at the southernmost stations of the AESOPS 170° W cruises (Buesseler et al., 2003). At reference station R-2, prevalence of Fe stress is indicated by the low dissolved Fe (DFe) levels in the surface (~ 0.1 $nmol\,L^{-1}$; Queroue et al., 2014) and also by Fe limitation of phytoplankton growth evidenced from deck board incubations (Bowie et al., 2014).

Carbon export decreased rapidly with depth at station R-2, and more than 50 % of EP100 was lost between 100 and 200 m depth. A similar trend was deduced from gel traps (Laurenceau et al., 2014). In our case, sharp decrease of export with depth seems to be essentially driven by the C : Th ratio of sinking particles, which decreases from 9.2 $\mu mol\,dpm^{-1}$ to 4.1 $\mu mol\,dpm^{-1}$ between 100 and 200 m (Fig. 5). Such a decrease may support a preferential loss of C relative to ^{234}Th due to a partial degradation of sinking particles (Buesseler et al., 2006). This feature could involve the heterotrophic bacterial activity, since high content of bacteria cells (2.9 10^5 $cell\,mL^{-1}$) are found between 100 and 150 m (Christaki et al., 2014).

4.2 North of Polar Front site (F-L)

Export production north of the PF at station F-L is low with 4.1 ± 0.6 $mmol\,m^{-2}\,d^{-1}$ at 100 m. EP100 in these iron-enriched waters is only 1.1-fold higher than at the control station R-2 and indicates no impact of Fe fertilization on upper-ocean carbon export in early bloom conditions. However, ^{234}Th export flux at F-L is 2.2 times higher in comparison to the reference station and indicates a more efficient scavenging of particles in the PFZ. This is supported further by the similar 100 m ^{234}Th flux observed in the same area at TEW-8 (886±162 $dpm\,m^{-2}\,d^{-1}$). It should be mentioned that EP100 at F-L may be underestimated because the C : Th ratio used to convert the ^{234}Th flux into C flux was taken at 130 m depth and may be lower than at 100 m depth. As an example, C : Th ratio of 1–53 µm particle at station F-L is 6.0 µmol dpm^{-1} at 70 m and strongly decreases to 4.5 µmol dpm^{-1} at 130 m. However, considering deeper export, EP200 at F-L (3.0 ± 0.8 mmol m^{-2} d^{-1}) appears 1.6-fold higher than at the reference station R suggesting an early impact of Fe fertilization on C export at 200 m depth. In this area, C export estimated using the ^{234}Th proxy shows excellent agreement with fluxes deduced from gel traps (Laurenceau et al., 2014).

The observed trend in carbon export drastically contrasts with the very high productivity at F-L. A massive bloom rapidly developed in early November in this area as revealed by satellite images (F. D'Ovidio, personal communication, 2013) and station F-L was occupied only a few days after the start of the bloom. Phytoplankton biomass was high with total Chl *a* up to 5.0 µg L^{-1}, total BSi up to 3.9 µmol L^{-1} and POC up to 28.2 µmol L^{-1} (Lasbleiz et al., 2014), with the diatom-dominated phytoplankton community in the fast-growing phase as revealed by Si (Closset et al., 2014) and C (Cavagna et al., 2014) uptake rates. The phytoplankton community was composed of a broad spectrum of size and taxa with small species presumably originating from Fe-rich waters of the northern Kerguelen shelf, and large species being characteristic of low biomass waters south of the PF offshore of the island (Trull et al., 2014). It is interesting to note that high biomass content is reflected in the partition of ^{234}Th showing very high $^{234}Th_p$ activity (0.9 dpm L^{-1} at 40 m, see Fig. 3). Furthermore, $^{234}Th_p$ appears to be evenly distributed among small and large particles similarly to phytoplankton community structure. Between 40 and 70 m depth, 40 % of $^{234}Th_p$ is found with the small (1–53 µm) particles and 60 % with the large (> 53 µm) particles. This size spectrum of particles clearly offers higher potential for C export at F-L compared to the HNLC reference station. However, comparison with NPP reveals that export efficiency is very low at F-L with a ThE ratio of 1.4 %. This clearly supports an inefficient transfer of C to depth and indicates a pronounced decoupling between export and production. Very low ThE ratio suggests that biomass is in accumulation phase and a major export event is likely to be delayed until later in the season.

BGD
11, 15991–16032, 2014

Comparison with literature data shows that EP100 at F-L ($4.1 \pm 0.6\,\text{mmol}\,\text{m}^{-2}\,\text{d}^{-1}$) remains substantially lower than C export flux reported during CROZEX experiment both during leg 1 (range 4.9–17 $\text{mmol}\,\text{m}^{-2}\,\text{d}^{-1}$) and leg 2 (13–30.0 $\text{mmol}\,\text{m}^{-2}\,\text{d}^{-1}$), even though similar Fe-rich waters of the PFZ were sampled.

Attenuation of export production with depth is relatively weak at F-L, as only 25 % of EP100 is lost between 100 and 200 m depth. This decrease is due to the decreasing C : Th ratio of sinking particles from 4.5 to 3.1 $\mu\text{mol}\,\text{dpm}^{-1}$ between 130 and 200 m. As already mentioned for the reference site, this trend may involve heterotrophic degradation of sinking particles. However, bacterial production at F-L is most intense in the first 60 m and decreases rapidly with depth to reach values similar to the reference station below 100 m depth (Christaki et al., 2014). At F-L, large particles seems to be more resistant to heterotrophic degradation and this may be linked to the higher abundance of fast-sinking cylindrical fecal pellets (Laurenceau et al., 2014).

4.3 Plateau site A3

Station A3 was located in iron- and silicic acid-rich waters over the central plateau and was visited twice, early (20 October) and late (16 November) during the survey. During the first and second visits very limited 100 m carbon export was observed, with 3.5 ± 0.9 and $4.6 \pm 1.5\,\text{mmol}\,\text{m}^{-2}\,\text{d}^{-1}$ at A3-1 and A3-2 respectively, based on the SS model. Based on the NSS model, the 100 m carbon export at A3-2 appears slightly higher with $7.3 \pm 1.8\,\text{mmol}\,\text{m}^{-2}\,\text{d}^{-1}$. EP100 at A3 shows no difference or a maximum of 1.9-fold higher flux in comparison to the HNLC reference station suggesting limited impact of Fe fertilization. It is interesting to note that the ^{234}Th deficit follows the density structure and extends to the bottom of the mixed layer at 150–200 m. This is much deeper than at stations R-2 or F-L, and consequently ^{234}Th export flux increases to $776 \pm 171\,\text{dpm}\,\text{m}^{-2}\,\text{d}^{-1}$ at A3-1 and to $993 \pm 200\,\text{dpm}\,\text{m}^{-2}\,\text{d}^{-1}$ at A3-2 between 100 and 200 m depth. At A3-2, carbon export was the highest at 150 m depth with 7.1 ± 1.5 and $8.4 \pm 1.8\,\text{mmol}\,\text{m}^{-2}\,\text{d}^{-1}$ based on SS and NSS model respectively, and is 2.8 to

BGD
11, 15991–16032, 2014

3.4 fold-higher in comparison to the HNLC station. At 200 m, increasing ^{234}Th export is cancelled by the simultaneous decrease of C : Th ratios resulting in low carbon export similar to A3-1. Comparison of sediment and gel traps can be conducted at A3-2. First, we observe an excellent agreement between ISP and sediment trap C : Th ratios (Fig. 6) indicating that the choice of large (> 53 µm) particles collected via ISP as representative of sinking particles was appropriate. Second, 200 m export fluxes estimated in this study (3.1 ± 0.6 and 3.8 ± 0.8 mmol m^{-2} d^{-1} with SS and NSS model, respectively) compare well with sediment trap flux (2.2 ± 0.7 mmol m^{-2} d^{-1}) and are smaller than gel trap-derived fluxes (5.5 mmol m^{-2} d^{-1}). The low flux sampled with the sediment trap may indicate undertrapping, but given that the trap was deployed only for one day, this site is particularly susceptible to temporal mismatch resulting from short-term variations in particle fluxes. However, it is worth mentioning that the good agreement found between the different and totally independent approaches is encouraging and tends to confirm that export production over the central plateau was rather low throughout the survey.

Low export production at A3 contrasts with the rapid biomass increase that occurred a few days before the second visit as revealed by satellite images (F. D'Ovidio, personal communication, 2013). The phytoplankton bloom at A3 showed different characteristics compared to station F-L suggesting variable biological responses to Fe fertilization. The bloom over the central plateau was dominated by fast-growing, large and heavily-silicified diatoms (Trull et al., 2014) showing very high Si uptake rates (Closset et al., 2014). The change in biomass levels at A3 is well reproduced by ^{234}Th$_p$ activity increasing from 0.25 to 0.55 dpm L^{-1} between the first and the second visit. These changes are observed also in the size partitioning of ^{234}Th$_p$. While at A3-1, 95 % of ^{234}Th$_p$ is found associated with small (1–53 µm) particles, at A3-2 ~ 70 % is found with large (> 53 µm) particles between 55 and 165 m depth. This clearly suggests a very high potential for export at A3-2, although massive export event had not yet commenced. Delayed export is suggested further by the very low ThE ratio at A3-2 (3 to

5 % depending on scavenging model), which indicates that biomass was accumulating in the mixed layer.

Over the central plateau, carbon export during the early stages of the bloom (range: 3.1 ± 0.6–$3.8\pm0.8\,\mathrm{mmol\,m^{-2}\,d^{-1}}$ at 200 m depth) are 4.4 to 12 times smaller than during the KEOPS1 late summer condition (13.9 ± 5.9–$37.7\pm13.3\,\mathrm{mmol\,m^{-2}\,d^{-1}}$ at 200 m depth) (Savoye et al., 2008). This difference is essentially due to much higher ^{234}Th fluxes reported during KEOPS1 (range 2249 ± 772–$8016\pm949\,\mathrm{dpm\,m^{-2}\,d^{-1}}$) indicating that particle scavenging is much more intense in January–February during the peak and decline of the bloom. Interestingly, the C : Th ratio of sinking particles exhibits a similar range over the entire growth season, 3.1–9.9 $\mathrm{\mu mol\,dpm^{-1}}$ during KEOPS1 and 4.7–7.7 $\mathrm{\mu mol\,dpm^{-1}}$ during KEOPS-2, between 100 and 200 m depth. This is relatively surprising because sinking particles are very different between the early and late bloom period over the plateau. During KEOPS2, sinking particles were dominantly composed of phytodetrital aggregates (Laurenceau et al., 2014) and rapid aggregation of diatom cells was also evidenced from underwater vision profiler observations and modeling (Jouandet et al., 2014). During KEOPS1, the export process was different and the majority of the particle flux (composed of fecal pellets and fecal aggregates) was processed through the heterotrophic food web (Ebersbach and Trull, 2008).

4.4 PF meander site E

Export production in the recirculation feature south of the PF (stations E) was the highest during the whole survey (Fig. 6). The four visits carried out as a pseudo-lagrangian survey (E-1, E-3, E-4E, and E-5) revealed the short-term temporal variability of carbon export over 19.6 days in moderately iron-enriched waters (Queroue et al., 2014; Bowie et al., 2014). The carbon export at 100 m was particularly elevated at the first ($11.6\pm1.3\,\mathrm{mmol\,m^{-2}\,d^{-1}}$, E-1) and at the second visit ($11.8\pm1.1\,\mathrm{mmol\,m^{-2}\,d^{-1}}$, E-3), and decreased progressively at the third ($5.4\pm0.7\,\mathrm{mmol\,m^{-2}\,d^{-1}}$, E-4E) and fourth ($7.7\pm1.3\,\mathrm{mmol\,m^{-2}\,d^{-1}}$, E-5) visits. A comparison with the reference station indicates 3- to 1.4-fold enhanced export within the recirculation feature suggesting an early impact

BGD
11, 15991–16032, 2014

of Fe fertilization on the carbon flux at 100 m depth. High export appears primarily influenced by an elevated 100 m ^{234}Th flux, ranging between 1051 ± 121 dpm m^{-2} d^{-1} and 1326 ± 110 dpm m^{-2} d^{-1}. Note that high ^{234}Th export was also observed in the same area earlier in the survey (21–22 October) at transect stations TNS-6 and TNS-8. These results support an early export event in the PF meander that had occurred before the start of the bloom and was associated with moderate biomass levels. The integrated total Chl *a* stocks at 200 m were relatively stable with 141 mg m^{-2} at E-1, 112 mg m^{-2} at E-2, 96 mg m^{-2} at E-3, 108 mg m^{-2} at E-4E, and 126 mg m^{-2} at E-5 (Lasbleiz et al., 2014). Furthermore, the relatively constant ^{234}Th flux over the 19 day period may indicate that particle scavenging is at steady state, i.e. constant export (Savoye et al., 2006). This is supported also by the excellent agreement found between SS and NSS estimates of 100 m ^{234}Th fluxes at E-4E and E-5 (Table 1). However, local variation in ^{234}Th distribution seems to exist in the PF meander as seen with the smaller ^{234}Th flux recorded at station E-2 which was part of the west to east transect (TEW) (Fig. 6). The smaller deficit at this station may have been caused by lateral advection of ^{234}Th-rich (lower deficit) waters originating from the jet of the PF passing to the north. The second controlling factor of 100 m carbon export was the sinking particles C : Th ratio, showing elevated values at E-1 (10.5 ± 0.2 µmol dpm^{-1}) and E-3 (8.9 ± 0.3 µmol dpm^{-1}) decreasing progressively at E-4E (5.1 ± 0.3 µmol dpm^{-1}) and E-5 (6.1 ± 0.2 µmol dpm^{-1}). As already mentioned, such a decrease may indicate preferential loss of carbon relative to ^{234}Th (Buesseler et al., 2006). This may involve food web interactions including bacterial production in the mixed layer increasing from 30 nmol C L^{-1} d^{-1} (E-1) to 54.7 nmol C L^{-1} d^{-1} (E-5) (Christaki et al., 2014) as well as grazing activity by zooplankton (Carlotti et al., 2014).

The carbon export at 200 m was also elevated in the recirculation feature (range: 5.3 ± 1.0 to 8.2 ± 0.8 mmol m^{-2} d^{-1}) but shows less temporal variability. High 200 m carbon export results from a very deep ^{234}Th deficit extending down to 200 m depth, except at E-4E where the export depth is shallower (∼ 150 m). Consequently, important increases in ^{234}Th export (up to a factor of 2 at E-5) were observed between 100 and

200 m depth. This feature is not in line with the relatively shallow mixed layer depth estimated in the PF meander (range: 38–74 m depth) and seems to follow the depth of the winter mixed layer. Note that macronutrients (nitrate and silicic acid) and dissolved trace elements profiles (Queroue et al., 2014) display similar patterns as the ^{234}Th deficit. Such a vertical distribution suggests important vertical mixing in the area and tends to confirm that ^{234}Th export has occurred earlier in the survey. The ^{234}Th export at 200 m displays little variability over the 19.6 days of sampling and this feature is also observed in sediment traps deployed at E-1, E-3 and E-5, even though the traps have collected ~ 50 % of the flux deduced from ^{234}Th deficit. The C : Th ratio in sinking particles decreases sharply between 100 and 200 m depth at E-1 and E-3 and to a lesser extent at E-4E and E-5 (Fig. 6). Ratios estimated from ISP show very good agreement with trap C : Th ratios at E-3 and E-5 but not at E-1. The trap C : Th ratio at E-1 was highly variable (8.6 ± 3.9 µmol dpm^{-1}) and appears closer to C : Th ratios of small (1–53 µm) particles, suggesting a potential contribution of these particles to the overall export. A decreasing C : Th ratio results in lower carbon export at 200 m compared with 100 m. However, a comparison with the HNLC reference station reveals between 2.9 and 4.5-fold higher carbon fluxes in the PF meander at 200 m depth. This suggests a strong impact of Fe fertilization in this area which is subjected to moderate dissolved Fe inputs. The impact of Fe fertilization on carbon export at this location is of similar magnitude compared to the KEOPS1 study (Savoye et al., 2008).

High export production in the PF meander remains relatively unexpected considering the temporal variation of surface phytoplankton community structure. Initially dominated by small size particles including small centric and pennate diatoms, the larger phytoplankton fraction increased progressively and became dominant at the end of the time series (E-5) (Trull et al., 2014). This variability is also observed in ^{234}Th$_p$ and POC partitioning between the surface and 150 m depth. At E1, E-3, and E-4E, small particles represent the dominant fraction of ^{234}Th$_p$ and POC with 60 up to 80 %, while at E-5 small particles fraction decreases to 50 %. This suggests an increasing potential for export, whereas export production tends to decrease with time. The same feature

BGD
11, 15991–16032, 2014

is observed for C (Cavagna et al., 2014) and Si uptake rates (Closset et al., 2014) showing low productivity at the beginning increasing progressively during the course of the survey. These inverse temporal variations between export and production are supported further by the ThE ratio, where high values were observed initially (27 %) at E-1 decreasing progressively until E-5 (6 %). The reason for this decoupling may be numerous and highlights the complexity of export processes that cannot be easily resolved based only on primary production variability. One hypothesis may involve food web interactions through grazing pressure, since fecal material is one of the main carriers of the POC export in the upper 200 m at the E stations (Laurenceau et al., 2014).

The early bloom export production in the PF meander can be compared to the late summer situation reported for station A11 during KEOPS1 located in similar deep waters east of Kerguelen Island (Savoye et al., 2008). Carbon export at A11 in late summer (range: 19.4–26.3 $\mathrm{mmol\,m^{-2}\,d^{-1}}$) is substantially higher than EP100 (range: 5.4–11.6 $\mathrm{mmol\,m^{-2}\,d^{-1}}$) and EP200 (5.3–7.7 $\mathrm{mmol\,m^{-2}\,d^{-1}}$) at stations E confirming that an important fraction of the seasonal export was not sampled during KEOPS2. At A11, the C : Th ratio was 11.0 ± 1.2 and 6.3 $\mathrm{\mu mol\,dpm^{-1}}$ at 100 and 200 m depth, respectively, and appears very close to the C : Th ratios measured at E-1 and E-3, and higher than the ratios measured at E-4E and E-5.

5 Conclusions

In the present study, we investigated upper-ocean carbon export production in the naturally Fe-fertilized area adjacent to Kerguelen Island as part of the KEOPS2 expedition. Spatial and temporal variations in water-column total ^{234}Th activity combined with the C : Th ratios of large potentially sinking particles were used to infer carbon export between 100 and 200 m depth. Export production in the Fe-fertilized area reveals large spatial variability during the early stages of bloom development with low export found at high productivity sites located over the central plateau (A3 site) and north of the PF in deep water downstream of the island (F-L site). Highest export was observed south of the permanent meander of the PF (E stations) where a detailed time series was obtained as part of a pseudo-lagrangian study. The comparison with the HNLC reference station located south of the PF and upstream of the island, indicates that Fe fertilization increased carbon export in all iron fertilized waters during the early stage of the Kerguelen bloom but at variable degrees. The increase is particularly significant inside the PF meander, but more moderate over the central Kerguelen plateau and in the northern plume of the Kerguelen bloom. Export efficiencies were particularly low at high productivity sites over and off the plateau (A3 and F-L sites) and clearly indicate that biomass was in accumulation phase rather than in export phase. The varied response of ecosystems to natural iron inputs results in varied phytoplankton community size structures, which in turn impacts the potential for carbon export. The highest carbon export potential was observed over the central plateau (station A3) showing high biomass dominated by large diatoms. Comparison with late summer export production obtained during KEOPS1 reveals a much smaller carbon flux during the early stages of the bloom in spring than in late summer.

The Supplement related to this article is available online at doi:10.5194/bgd-11-15991-2014-supplement.

Acknowledgements. We are grateful to KEOPS2 chief scientists Stéphane Blain and Bernard Quéguiner, and to the Captain and crew of R/V *Marion Dufresne* for their assistance and help during the cruise. This research was supported by the French Agency of National Research (grant: #ANR-10-BLAN-0614), the Program LEFE-CYBER of Institut des Sciences de l'Univers (INSU), the Institut Paul Emile Victor. Financial supports were obtained from Belgian Science Policy (BELSPO, grant SD/CA/05A), Flanders Research Foundation (FWO, grant G071512N), Vrije Universiteit Brussel (Strategic Research Plan), the Antarctic Climate and Ecosystem Cooperative Research Center (ACE-CRC, Hobart, Australia). We are very grateful to Michael Korntheuer for state of the art beta counter maintenance, Jacques Navez and Laurence Monin for helpful laboratory assistance. We would to thank Lionel Scouarnec, Anne Royer, and Fabien Perault from the Technical Division of INSU in Brest for their assistance during the cruise.

References

Alderkamp, A.-C., Mills, M. M., van Dijken, G. L., Laan, P., Thuróczy, C.-E., Gerringa, L. J. A., de Baar, H. J. W., Payne, C. D., Visser, R. J. W., Buma, A. G. J., and Arrigo, K. R.: Iron from melting glaciers fuels phytoplankton blooms in the Amundsen Sea (Southern Ocean): phytoplankton characteristics and productivity, Deep-Sea Res. Pt. II, 71–76, 32–48, 2012.

Blain, S., Queguiner, B., Armand, L., Belviso, S., Bombled, B., Bopp, L., Bowie, A., Brunet, C., Brussaard, C., Carlotti, F., Christaki, U., Corbiere, A., Durand, I., Ebersbach, F., Fuda, J.-L., Garcia, N., Gerringa, L., Griffiths, B., Guigue, C., Guillerm, C., Jacquet, S., Jeandel, C., Laan, P., Lefevre, D., Lo Monaco, C., Malits, A., Mosseri, J., Obernosterer, I., Park, Y.-H., Picheral, M., Pondaven, P., Remenyi, T., Sandroni, V., Sarthou, G., Savoye, N., Scouarnec, L., Souhaut, M., Thuiller, D., Timmermans, K., Trull, T., Uitz, J., van Beek, P., Veldhuis, M., Vincent, D., Viollier, E., Vong, L., and Wagener, T.: Effect of natural iron fertilization on carbon sequestration in the Southern Ocean, Nature, 446, 1070–1074, 2007.

Blain, S., Sarthou, G., and Laan, P.: Distribution of dissolved iron during the natural iron-fertilization experiment KEOPS (Kerguelen Plateau, Southern Ocean), Deep-Sea Res. Pt. II, 55, 594–605, 2008.

Blain, S., Capparos, J., Guéneuguès, A., Obernosterer, I., and Oriol, L.: Distributions and stoichiometry of dissolved nitrogen and phosphorus in the iron fertilized region near Kerguelen (Southern Ocean), Biogeosciences Discuss., 11, 9949–9977, doi:10.5194/bgd-11-9949-2014, 2014.

Borrione, I. and Schlitzer, R.: Distribution and recurrence of phytoplankton blooms around South Georgia, Southern Ocean, Biogeosciences, 10, 217–231, doi:10.5194/bg-10-217-2013, 2013.

Bowie, A. R., Townsend, A. T., Lannuzel, D., Remenyi, T. A., and van der Merwe, P.: Modern sampling and analytical methods for the determination of trace elements in marine particulate material using magnetic sector inductively coupled plasma–mass spectrometry, Anal. Chim. Acta, 676, 15–27, 2010.

Boyd, P. W., Watson, A. J., Law, C. S., Abraham, E. R., Trull, T., Murdoch, R., Bakker, D. C. E., Bowie, A. R., Buesseler, K. O., Chang, H., Charette, M., Croot, P., Downing, K., Frew, R., Gall, M., Hadfield, M., Hall, J., Harvey, M., Jameson, G., LaRoche, J., Liddicoat, M., Ling, R., Maldonado, M. T., McKay, R. M., Nodder, S., Pickmere, S., Pridmore, R., Rintoul, S., Safi, K., Sutton, P., Strzepek, R., Tanneberger, K., Turner, S., Waite, A., and Zeldis, J.: A mesoscale phytoplankton bloom in the polar Southern Ocean stimulated by iron fertilization, Nature, 407, 695–702, 2000.

Boyd, P. W., Jickells, T., Law, C. S., Blain, S., Boyle, E. A., Buesseler, K. O., Coale, K. H., Cullen, J. J., de Baar, H. J. W., Follows, M., Harvey, M., Lancelot, C., Levasseur, M., Owens, N. P. J., Pollard, R., Rivkin, R. B., Sarmiento, J., Schoemann, V., Smetacek, V., Takeda, S., Tsuda, A., Turner, S., and Watson, A. J.: Mesoscale iron enrichment experiments 1993–2005: synthesis and future directions, Science, 315, 612–617, 2007.

Buesseler, K. O.: The decoupling of production and particulate export in the surface ocean, Global Biogeochem. Cy., 12, 297–310, 1998.

Buesseler, K. O., Bacon, M. P., Kirk Cochran, J., and Livingston, H. D.: Carbon and nitrogen export during the JGOFS North Atlantic Bloom experiment estimated from ^{234}Th : ^{238}U disequilibria, Deep-Sea Res. Pt. I, 39, 1115–1137, 1992.

Buesseler, K. O., Ball, L., Andrews, J., Cochran, J. K., Hirschberg, D. J., Bacon, M. P., Fleer, A., and Brzezinski, M.: Upper ocean export of particulate organic carbon and biogenic silica in the Southern Ocean along 170° W, Deep-Sea Res. Pt. II, 48, 4275–4297, 2001.

Buesseler, K. O., Barber, R. T., Dickson, M.-L., Hiscock, M. R., Moore, J. K., and Sambrotto, R.: The effect of marginal ice-edge dynamics on production and export in the Southern Ocean along 170° W, Deep-Sea Res. Pt. II, 50, 579–603, 2003.

Buesseler, K., Andrews, J., Pike, S., and Charette, M.: The effects of iron fertilization on carbon sequestration in the Southern Ocean, Science, 304, 414–417, 2004.

Buesseler, K., Andrews, J., Pike, S. M., Charette, M. A., Goldson, L. E., Brzezinski, M. A., and Lance, V. P.: Particle export during the Southern Ocean Iron Experiment (SOFeX), Limnol. Oceanogr., 50, 311–327, 2005.

Buesseler, K. O., Benitez-Nelson, C. R., Moran, S. B., Burd, A., Charette, M., Cochran, J. K., Coppola, L., Fisher, N. S., Fowler, S. W., Gardner, W. D., Guo, L. D., Gustafsson, Ã., Lamborg, C., Masque, P., Miquel, J. C., Passow, U., Santschi, P. H., Savoye, N., Stewart, G., and Trull, T.: An assessment of particulate organic carbon to thorium-234 ratios in the ocean

BGD
11, 15991–16032, 2014

and their impact on the application of ^{234}Th as a POC flux proxy, Mar. Chem., 100, 213–233, 2006.

Christaki, U., Lefèvre, D., Georges, C., Colombet, J., Catala, P., Courties, C., Sime-Ngando, T., Blain, S., and Obernosterer, I.: Microbial food web dynamics during spring phytoplankton blooms in the naturally iron-fertilized Kerguelen area (Southern Ocean), Biogeosciences Discuss., 11, 6985–7028, doi:10.5194/bgd-11-6985-2014, 2014.

Closset, I., Lasbleiz, M., Leblanc, K., Quéguiner, B., Cavagna, A.-J., Elskens, M., Navez, J., and Cardinal, D.: Seasonal evolution of net and regenerated silica production around a natural Fe-fertilized area in the Southern Ocean estimated with Si isotopic approaches, Biogeosciences, 11, 5827–5846, doi:10.5194/bg-11-5827-2014, 2014.

Coale, K. H., Johnson, K. S., Chavez, F. P., Buesseler, K. O., Barber, R. T., Brzezinski, M. A., Cochlan, W. P., Millero, F. J., Falkowski, P. G., Bauer, J. E., Wanninkhof, R. H., Kudela, R. M., Altabet, M. A., Hales, B. E., Takahashi, T., Landry, M. R., Bidigare, R. R., Wang, X., Chase, Z., Strutton, P. G., Friederich, G. E., Gorbunov, M. Y., Lance, V. P., Hilting, A. K., Hiscock, M. R., Demarest, M., Hiscock, W. T., Sullivan, K. F., Tanner, S. J., Gordon, R. M., Hunter, C. N., Elrod, V. A., Fitzwater, S. E., Jones, J. L., Tozzi, S., Koblizek, M., Roberts, A. E., Herndon, J., Brewster, J., Ladizinsky, N., Smith, G., Cooper, D., Timothy, D., Brown, S. L., Selph, K. E., Sheridan, C. C., Twining, B. S., and Johnson, Z. I.: Southern Ocean Iron Enrichment Experiment: carbon cycling in high- and low-Si waters, Science, 304, 408–414, 2004.

Cochran, J. K. and Masqué, P.: Short-lived U/Th series radionuclides in the ocean: tracers for scavenging rates, export fluxes and particle dynamics, Rev. Mineral. Geochem., 52, 461–492, 2003.

Cochran, J. K., Buesseler, K. O., Bacon, M. P., Wang, H. W., Hirschberg, D. J., Ball, L., Andrews, J., Crossin, G., and Fleer, A.: Short-lived thorium isotopes (^{234}Th, ^{228}Th) as indicators of POC export and particle cycling in the Ross Sea, Southern Ocean, Deep-Sea Res. Pt. II, 47, 3451–3490, 2000.

Ebersbach, F. and Trull, T. W.: Sinking particle properties from polyacrylamide gels during the KErguelen Ocean and Plateau compared Study (KEOPS): zooplankton control of carbon export in an area of persistent natural iron inputs in the Southern Ocean, Limnol. Oceanogr., 53, 212–224, 2008.

Jacquet, S. H. M., Savoye, N., Dehairs, F., Strass, V. H., and Cardinal, D.: Mesopelagic carbon remineralization during the European Iron Fertilization Experiment, Global Biogeochem. Cy., 22, GB1023, doi:10.1029/2006GB002902, 2008.

Jouandet, M. P., Blain, S., Metzl, N., Brunet, C., Trull, T. W., and Obernosterer, I.: A seasonal carbon budget for a naturally iron-fertilized bloom over the Kerguelen Plateau in the Southern Ocean, Deep-Sea Res. Pt. II, 55, 856–867, 2008.

Jouandet, M.-P., Jackson, G. A., Carlotti, F., Picheral, M., Stemmann, L., and Blain, S.: Rapid formation of large aggregates during the spring bloom of Kerguelen Island: observations and model comparisons, Biogeosciences, 11, 4393–4406, doi:10.5194/bg-11-4393-2014, 2014.

Lasbleiz, M., Leblanc, K., Blain, S., Ras, J., Cornet-Barthaux, V., Hélias Nunige, S., and Quéguiner, B.: Pigments, elemental composition (C, N, P, Si) and stoichiometry of particulate matter, in the naturally iron fertilized region of Kerguelen in the Southern Ocean, Biogeosciences Discuss., 11, 8259–8324, doi:10.5194/bgd-11-8259-2014, 2014.

Laurenceau, E. C., Trull, T. W., Davies, D. M., Bray, S. G., Doran, J., Planchon, F., Carlotti, F., Jouandet, M.-P., Cavagna, A.-J., Waite, A. M., and Blain, S.: The relative importance of phytoplankton aggregates and zooplankton fecal pellets to carbon export: insights from free-drifting sediment trap deployments in naturally iron-fertilised waters near the Kerguelen plateau, Biogeosciences Discuss., 11, 13623–13673, doi:10.5194/bgd-11-13623-2014, 2014.

Le Moigne, F. A. C., Henson, S. A., Sanders, R. J., and Madsen, E.: Global database of surface ocean particulate organic carbon export fluxes diagnosed from the ^{234}Th technique, Earth Syst. Sci. Data, 5, 295–304, doi:10.5194/essd-5-295-2013, 2013.

Lucas, M., Seeyave, S., Sanders, R., Mark Moore, C., Williamson, R., and Stinchcombe, M.: Nitrogen uptake responses to a naturally Fe-fertilised phytoplankton bloom during the 2004/2005 CROZEX study, Deep-Sea Res. Pt. II, 54, 2138–2173, 2007.

Martin, J. H.: Glacial–interglacial CO_2 change: the Iron Hypothesis, Paleoceanography, 5, 1–13, 1990.

Martin, J. H., Fitzwater, S. E., and Gordon, R. M.: Iron deficiency limits phytoplankton growth in Antarctic waters, Global Biogeochem. Cy., 4, 5–12, 1990.

Martin, J. H., Gordon, R. M., and Fitzwater, S. E.: The case for iron, Limnol. Oceanogr., 36, 1793–1802, 1991.

Martin, P., van der Loeff, M. R., Cassar, N., Vandromme, P., d'Ovidio, F., Stemmann, L., Rengarajan, R., Soares, M., González, H. E., Ebersbach, F., Lampitt, R. S., Sanders, R., Barnett, B. A., Smetacek, V., and Naqvi, S. W. A.: Iron fertilization enhanced net community production but not downward particle flux during the Southern Ocean iron fertilization experiment LOHAFEX, Global Biogeochem. Cy., 27, 871–881, 2013.

Mongin, M., Molina, E., and Trull, T. W.: Seasonality and scale of the Kerguelen plateau phytoplankton bloom: a remote sensing and modeling analysis of the influence of natural iron fertilization in the Southern Ocean, Deep-Sea Res. Pt. II, 55, 880–892, 2008.

Moore, C. M., Mills, M. M., Arrigo, K. R., Berman-Frank, I., Bopp, L., Boyd, P. W., Galbraith, E. D., Geider, R. J., Guieu, C., Jaccard, S. L., Jickells, T. D., La Roche, J., Lenton, T. M., Mahowald, N. M., Maranon, E., Marinov, I., Moore, J. K., Nakatsuka, T., Oschlies, A., Saito, M. A., Thingstad, T. F., Tsuda, A., and Ulloa, O.: Processes and patterns of oceanic nutrient limitation, Nat. Geosci., 6, 701–710, 2013.

Morris, P. J., Sanders, R., Turnewitsch, R., and Thomalla, S.: ^{234}Th-derived particulate organic carbon export from an island-induced phytoplankton bloom in the Southern Ocean, Deep-Sea Res. Pt. II, 54, 2208–2232, 2007.

Mosseri, J., Quéguiner, B., Armand, L., and Cornet-Barthaux, V.: Impact of iron on silicon utilization by diatoms in the Southern Ocean: a case study of Si/N cycle decoupling in a naturally iron-enriched area, Deep-Sea Res. Pt. II, 55, 801–819, 2008.

Nodder, S. D., Charette, M. A., Waite, A. M., Trull, T. W., Boyd, P. W., Zeldis, J., and Buesseler, K. O.: Particle transformations and export flux during an in situ iron-stimulated algal bloom in the Southern Ocean, Geophys. Res. Lett., 28, 2409–2412, 2001.

Owens, S. A., Buesseler, K. O., and Sims, K. W. W.: Re-evaluating the ^{238}U-salinity relationship in seawater: implications for the ^{238}U–^{234}Th disequilibrium method, Mar. Chem., 127, 31–39, 2011.

Park, Y.-H., Fuda, J.-L., Durand, I., and Naveira Garabato, A. C.:. Internal tides and vertical mixing over the Kerguelen Plateau, Deep-Sea Res. Pt. II, 55, 582–593, 2008a.

Park, Y.-H., Roquet, F., Durand, I., and Fuda, J.-L.: Large-scale circulation over and around the Northern Kerguelen Plateau, Deep-Sea Res. Pt. II, 55, 566–581, 2008b.

Park, Y.-H., Lee, J.-H., Durand, I., and Hong, C.-S.: Validation of the Thorpe scale-derived vertical diffusivities against microstructure measurements in the Kerguelen region, Biogeosciences Discuss., 11, 12137–12157, doi:10.5194/bgd-11-12137-2014, 2014.

Pike, S. M., Buesseler, K. O., Andrews, J., and Savoye, N.: Quantification of ^{234}Th recovery in small volume sea water samples by inductively coupled plasma-mass spectrometry, J. Radioanal. Nucl. Ch., 263, 355–360, 2005.

Planchon, F., Cavagna, A.-J., Cardinal, D., André, L., and Dehairs, F.: Late summer particulate organic carbon export and twilight zone remineralisation in the Atlantic sector of the Southern Ocean, Biogeosciences, 10, 803–820, doi:10.5194/bg-10-803-2013, 2013.

BGD
11, 15991–16032, 2014

Carbon export in the naturally iron-fertilized Kerguelen area of the Southern Ocean

F. Planchon et al.

Planquette, H., Statham, P. J., Fones, G. R., Charette, M. A., Moore, C. M., Salter, I., Nédélec, F. H., Taylor, S. L., French, M., Baker, A. R., Mahowald, N., and Jickells, T. D.: Dissolved iron in the vicinity of the Crozet Islands, Southern Ocean, Deep-Sea Res. Pt. II, 54, 1999–2019, 2007.

Pollard, R. T., Salter, I., Sanders, R. J., Lucas, M. I., Moore, C. M., Mills, R. A., Statham, P. J., Allen, J. T., Baker, A. R., Bakker, D. C. E., Charette, M. A., Fielding, S., Fones, G. R., French, M., Hickman, A. E., Holland, R. J., Hughes, J. A., Jickells, T. D., Lampitt, R. S., Morris, P. J., Nedelec, F. H., Nielsdottir, M., Planquette, H., Popova, E. E., Poulton, A. J., Read, J. F., Seeyave, S., Smith, T., Stinchcombe, M., Taylor, S., Thomalla, S., Venables, H. J., Williamson, R., and Zubkov, M. V.: Southern Ocean deep-water carbon export enhanced by natural iron fertilization, Nature, 457, 577–580, 2009.

Rutgers van der Loeff, M., Cai, P. H., Stimac, I., Bracher, A., Middag, R., Klunder, M. B., and van Heuven, S. M. A. C.: ^{234}Th in surface waters: distribution of particle export flux across the Antarctic Circumpolar Current and in the Weddell Sea during the GEOTRACES expedition ZERO and DRAKE, Deep-Sea Res. Pt. II, 58, 2749–2766, 2011.

Salter, I., Lampitt, R. S., Sanders, R., Poulton, A., Kemp, A. E. S., Boorman, B., Saw, K., and Pearce, R.: Estimating carbon, silica and diatom export from a naturally fertilised phytoplankton bloom in the Southern Ocean using PELAGRA: a novel drifting sediment trap, Deep-Sea Res. Pt. II, 54, 2233–2259, 2007.

Savoye, N., Benitez-Nelson, C., Burd, A. B., Cochran, J. K., Charette, M., Buesseler, K. O., Jackson, G. A., Roy-Barman, M., Schmidt, S., and Elskens, M.: ^{234}Th sorption and export models in the water column: a review, Mar. Chem., 100, 234–249, 2006.

Savoye, N., Trull, T. W., Jacquet, S. H. M., Navez, J., and Dehairs, F.: ^{234}Th-based export fluxes during a natural iron fertilization experiment in the Southern Ocean (KEOPS), Deep-Sea Res. Pt. II, 55, 841–855, 2008.

Sedwick, P. N., DiTullio, G. R., Hutchins, D. A., Boyd, P. W., Griffiths, F. B., Crossley, A. C., Trull, T. W., and Quéguiner, B.: Limitation of algal growth by iron deficiency in the Australian Subantarctic Region, Geophys. Res. Lett., 26, 2865–2868, 1999.

Seeyave, S., Lucas, M. I., Moore, C. M., and Poulton, A. J.: Phytoplankton productivity and community structure in the vicinity of the Crozet Plateau during austral summer 2004/2005, Deep-Sea Res. Pt. II, 54, 2020–2044, 2007.

Smetacek, V., Klaas, C., Strass, V. H., Assmy, P., Montresor, M., Cisewski, B., Savoye, N., Webb, A., d'Ovidio, F., Arrieta, J. M., Bathmann, U., Bellerby, R., Berg, G. M., Croot, P.,

BGD
11, 15991–16032, 2014

Carbon export in the naturally iron-fertilized Kerguelen area of the Southern Ocean

F. Planchon et al.

Gonzalez, S., Henjes, J., Herndl, G. J., Hoffmann, L. J., Leach, H., Losch, M., Mills, M. M., Neill, C., Peeken, I., Rottgers, R., Sachs, O., Sauter, E., Schmidt, M. M., Schwarz, J., Terbruggen, A., and Wolf-Gladrow, D.: Deep carbon export from a Southern Ocean iron-fertilized diatom bloom, Nature, 487, 313–319, 2012.

Trull, T. W., Davies, D. M., Dehairs, F., Cavagna, A.-J., Lasbleiz, M., Laurenceau, E. C., d'Ovidio, F., Planchon, F., Leblanc, K., Quéguiner, B., and Blain, S.: Chemometric perspectives on plankton community responses to natural iron fertilization over and downstream of the Kerguelen Plateau in the Southern Ocean, Biogeosciences Discuss., 11, 13841–13903, doi:10.5194/bgd-11-13841-2014, 2014.

Zhou, M., Zhu, Y., Measures, C. I., Hatta, M., Charette, M. A., Gille, S. T., Frants, M., Jiang, M., Greg Mitchell, B.: Winter mesoscale circulation on the shelf slope region of the southern Drake Passage, Deep-Sea Res. Pt. II, 90, 4–14, 2013.

Table 1. ^{234}Th and POC export fluxes and C : Th ratios of sinking particles estimated at 100, 150, and 200 m depth, and carbon export efficiency (ThE) at 100 m depth during KEOPS2. (Bold text indicates that non-steady state calculations were used).

Station	Date	Depth (m)	^{234}Th flux (dpm m^{-2} d^{-1})	C : Th (µmol dpm^{-1})	POC flux (mmol m^{-2} d^{-1})	ThE (%)
R-2	25 Oct	100	412 ± 134	9.2 ± 0.5	3.8 ± 1.2	34
R-2	25 Oct	150	448 ± 146	5.6 ± 0.4	2.5 ± 0.8	
R-2	25 Oct	200	449 ± 203	4.1 ± 0.5	1.8 ± 0.9	16
TNS-8	21 Oct	100	942 ± 183			
TNS-8	21 Oct	150	1247 ± 221			
TNS-8	21 Oct	200	1372 ± 255			
TNS-6	22 Oct	100	794 ± 203			
TNS-6	22 Oct	150	1152 ± 238			
TNS-6	22 Oct	200	1328 ± 259			
TNS-1	23 Oct	100	600 ± 203			
TNS-1	23 Oct	150	646 ± 239			
TNS-1	23 Oct	200	567 ± 252			
A3-1	20 Oct	100	509 ± 127	6.9 ± 0.7	3.5 ± 0.9	
A3-1	20 Oct	150	666 ± 140	5.8 ± 0.7	3.9 ± 0.9	
A3-1	20 Oct	200	776 ± 171	4.8 ± 0.5	3.7 ± 0.9	
A3-2	16 Nov	100	463 ± 151	9.9 ± 0.1	4.6 ± 1.5	3
A3-2	16 Nov	150	829 ± 169	8.6 ± 0.1	7.1 ± 1.5	
A3-2	16 Nov	200	993 ± 200	3.1 ± 0.1	3.1 ± 0.6	
A3-2 Trap	15–17 Nov	200	506 ± 21	4.5 ± 1.5	2.2 ± 0.7	
A3-2	**20 Oct–16 Nov**	**100**	**736 ± 186**	**9.9 ± 0.1**	**7.3 ± 1.8**	**5**
A3-2	**20 Oct–16 Nov**	**150**	**975 ± 209**	**8.6 ± 0.1**	**8.4 ± 1.8**	
A3-2	**20 Oct–16 Nov**	**200**	**1202 ± 247**	**3.1 ± 0.1**	**3.8 ± 0.8**	
TEW-8	2 Nov	100	886 ± 162			
TEW-8	2 Nov	150	1050 ± 199			
TEW-8	2 Nov	200	1131 ± 233			
F-L	6 Nov	100	902 ± 117	4.5 ± 0.4	4.1 ± 0.6	1
F-L	6 Nov	150	891 ± 164	4.1 ± 0.4	3.6 ± 0.8	
F-L	6 Nov	200	973 ± 207	3.1 ± 0.5	3.0 ± 0.8	

Table 1. Continued.

Station	Date	Depth (m)	^{234}Th flux ($dpm\,m^{-2}\,d^{-1}$)	C : Th ($\mu mol\,dpm^{-1}$)	POC flux ($mmol\,m^{-2}\,d^{-1}$)	ThE (%)
E-1	30 Oct	100	1111 ± 120	10.5 ± 0.2	11.6 ± 1.3	27
E-1	30 Oct	150	1504 ± 158	5.5 ± 0.2	8.3 ± 0.9	
E-1	30 Oct	200	1665 ± 201	4.7 ± 0.2	7.7 ± 1.0	
E-1 Trap	29 Oct–3 Nov	200	881 ± 226	8.6 ± 3.9	7.0 ± 2.3	
E-2	1 Nov	100	664 ± 172			
E-2	1 Nov	150	921 ± 216			
E-2	1 Nov	200	1092 ± 253			
E-3	3 Nov	100	1326 ± 110	8.9 ± 0.3	11.8 ± 1.1	21
E-3	3 Nov	150	1742 ± 142	6.2 ± 0.2	10.8 ± 0.9	
E-3	3 Nov	200	1995 ± 176	4.1 ± 0.2	8.2 ± 0.8	
E-3 Trap	5 Nov–9 Nov	200	1129 ± 177	4.0 ± 0.7	4.9 ± 1.5	
E-4E	13 Nov	100	1051 ± 121	5.1 ± 0.3	5.4 ± 0.7	7
E-4E	13 Nov	150	1210 ± 155	3.3 ± 0.1	4.0 ± 0.5	
E-4E	13 Nov	200	1296 ± 193	4.1 ± 0.4	5.3 ± 1.0	
E-4E	**30 Oct–13 Nov**	**100**	**911 ± 242**	**5.1 ± 0.3**	**4.6 ± 1.3**	**6**
E-4E	**30 Oct–13 Nov**	**150**	**726 ± 315**	**3.3 ± 0.1**	**2.4 ± 1.0**	
E-4E	**30 Oct–13 Nov**	**200**	**525 ± 402**	**4.1 ± 0.4**	**2.1 ± 1.7**	
E-5	18 Nov	100	1262 ± 116	6.1 ± 0.1	7.7 ± 0.7	10
E-5	18 Nov	150	1671 ± 153	4.2 ± 0.2	7.0 ± 0.7	
E-5	18 Nov	200	1810 ± 190	3.7 ± 0.2	6.7 ± 0.8	
E-5 Trap	18 Nov–19 Nov	200	955 ± 546	2.4 ± 1.0	2.0 ± 1.0	
E-5	**30 Oct–18 Nov**	**100**	**1383 ± 177**	**6.1 ± 0.1**	**8.4 ± 1.1**	**11**
E-5	**30 Oct–18 Nov**	**150**	**1928 ± 235**	**4.2 ± 0.2**	**8.1 ± 1.0**	
E-5	**30 Oct–18 Nov**	**200**	**2034 ± 299**	**3.7 ± 0.2**	**7.5 ± 1.2**	
E-4W	11 Nov	100	1003 ± 124	6.7 ± 0.2	6.7 ± 0.9	3
E-4W	11 Nov	150	1174 ± 168	3.9 ± 0.1	4.5 ± 0.7	
E-4W	11 Nov	200	1068 ± 208	3.4 ± 0.2	3.7 ± 0.7	

BGD
11, 15991–16032, 2014

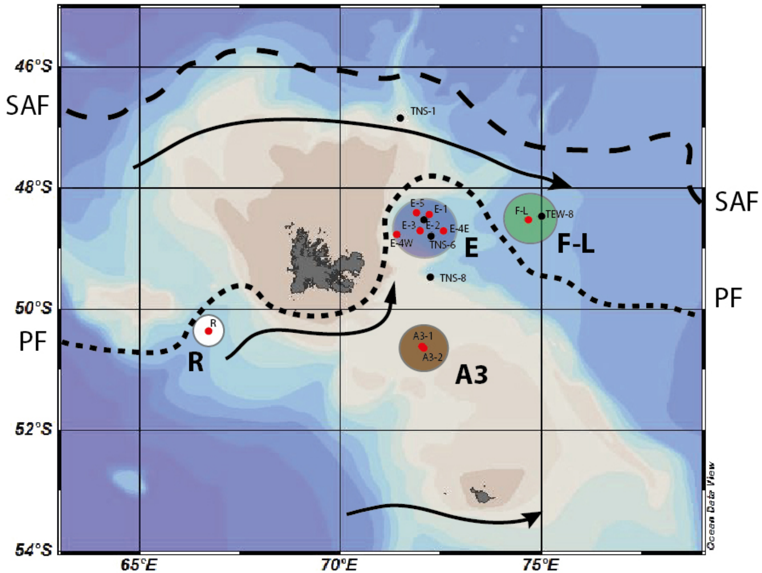

Figure 1. Stations map of ^{234}Th measurements during the KEOPS2 expedition. Also shown are the positions of the SubAntarctic Front (SAF) and the Polar Front (PF) adapted from Park et al. (2008b).

BGD
11, 15991–16032, 2014

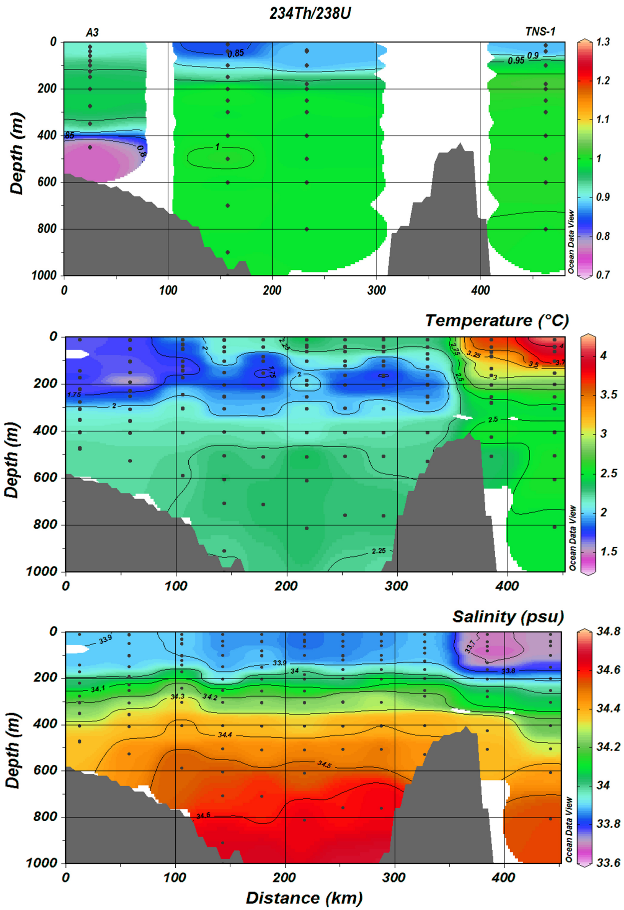

Figure 2. Latitudinal section of total $^{234}Th/^{238}U$ activity ratios, temperature and salinity obtained during the South to North transect from station A3 to station TNS-1. Schlitzer (2003); Ocean Data View; http://www.awi-bremerhaven.de/GEO/ODV.

BGD
11, 15991–16032, 2014

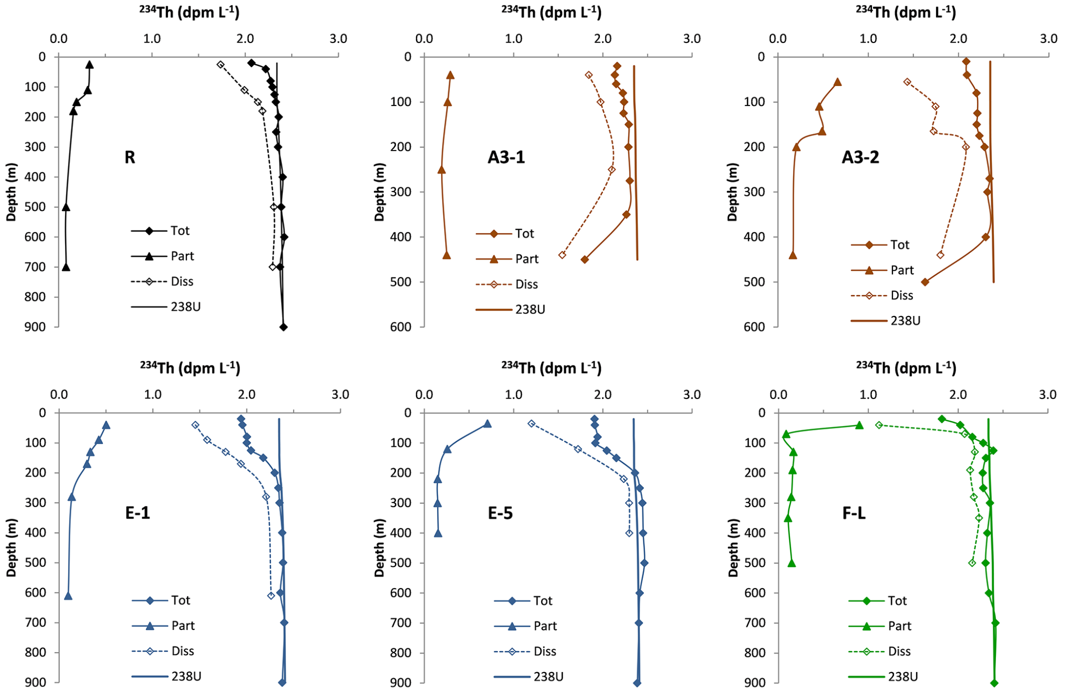

Figure 3. Depth profiles of total ^{234}Th ($^{234}Th_{tot}$), particulate $^{234}Th_p$ (sum of the two size fractions), and dissolved ^{234}Th (total – particulate, $^{234}Th_d$) activity (dpm L^{-1}) along with ^{238}U activity (dpm L^{-1}, solid lines) deduced from salinity at HNLC reference station R, central plateau station A3 (A3-1, first visit 20 October; A3-2, second visit 16 November), PF meander station E (E-1, first visit 30 October; E-5, fourth visit 8 November), and North of PF station F-L.

BGD
11, 15991–16032, 2014

Carbon export in the naturally iron-fertilized Kerguelen area of the Southern Ocean

F. Planchon et al.

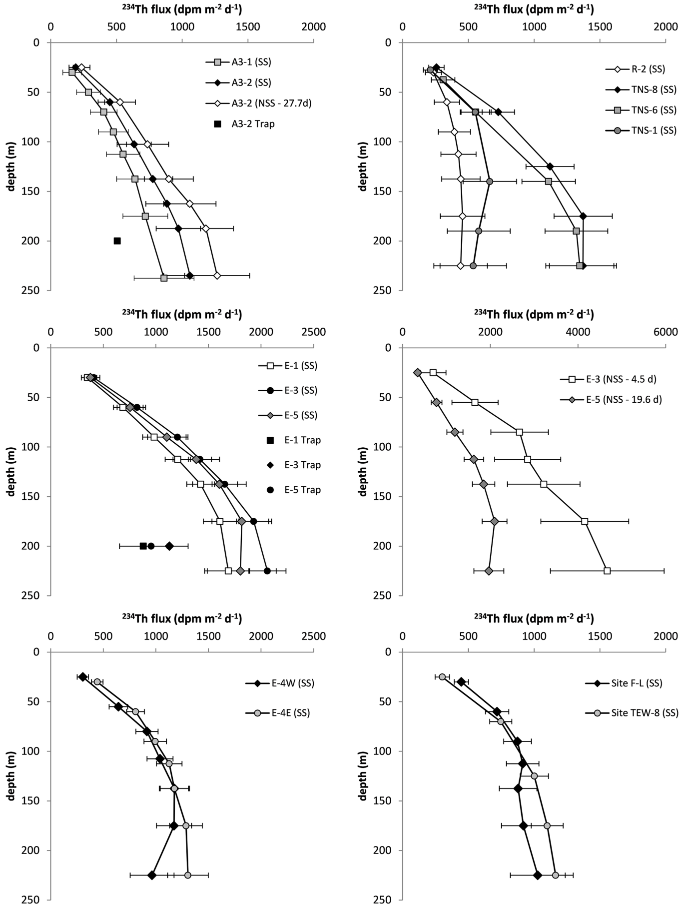

Figure 4. Depth profiles of cumulated total ^{234}Th export fluxes from the surface to 250 m depth using steady state (SS) and non-steady state (NSS) models and comparison with ^{234}Th export fluxes estimated from sediment traps at 200 m.

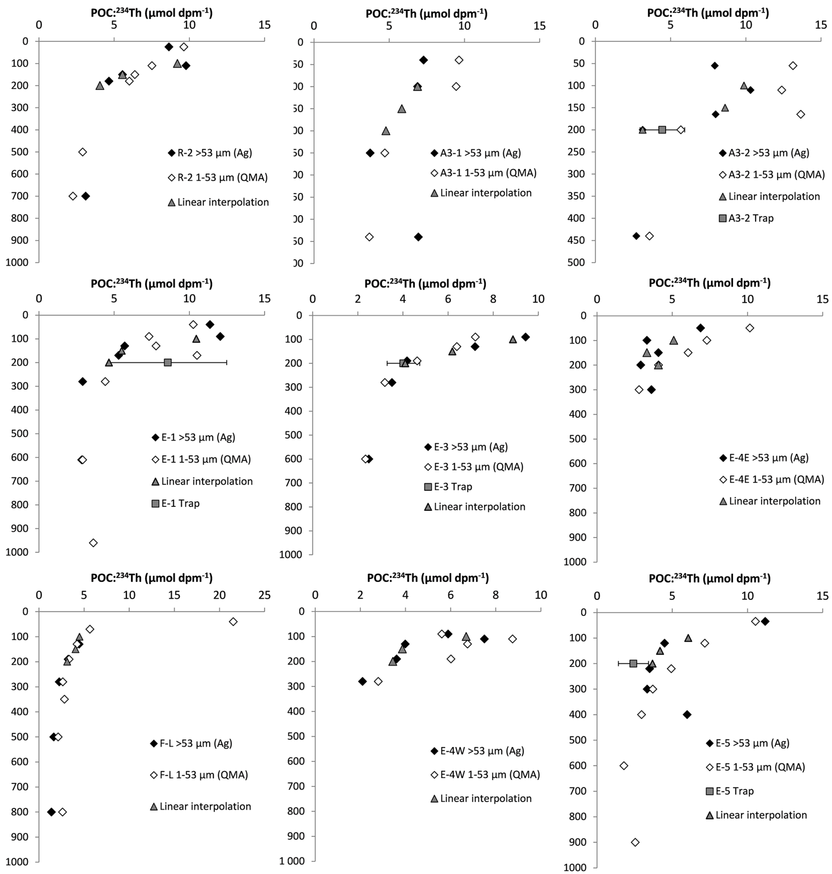

Figure 5. POC to ^{234}Th (C : Th) ratio in size-fractionated (1–53 and > 53 µm) suspended particulate matter collected by ISP and comparison with sinking particles collected via sediment traps at 200 m depth. Also shown is a linear interpolation of C : Th ratios at 100, 150, and 200 m depth for carbon flux estimates.

BGD
11, 15991–16032, 2014

Carbon export in the naturally iron-fertilized Kerguelen area of the Southern Ocean

F. Planchon et al.

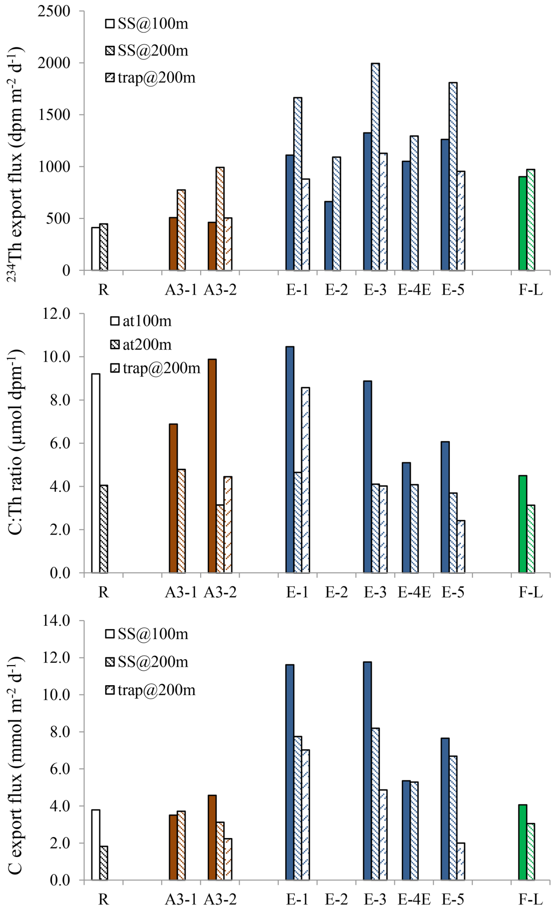

Figure 6. Summary results of ^{234}Th export fluxes (dpm m^{-2} d^{-1}), sinking particles C : Th ratios (µmol dpm^{-1}), and POC export fluxes (mmol m^{-2} d^{-1}) obtained at 100 and 200 m depth and comparison with sediment trap data obtained at 200 m depth during KEOPS2 survey.

BGD

11, 15991–16032, 2014

Carbon export in the naturally iron-fertilized Kerguelen area of the Southern Ocean

F. Planchon et al.